Trends in Atmospheric Sci., 1 (1992)

Dynamics of Madden-Julian Oscillation*

Bin Wang

Department of Meteorology,School of Ocean and Earth Science and Technology,University of Hawaii,2525 Correa Road, Honolulu,HI 96822,USA

Abstract

Madden-Julian Oscillation (MJO) is hypothesized to be a result of collective activity of planetary-scale tropical intraseasonal systems (TIS). This paper reviews theoretical studies of MJO, discusses various dynamic aspects of TIS, and presents some outstanding issues that require further investigations. In particular, a unified theoretical framework is proposed for study of the basic dynamics of TIS with which an Ekman-wave-CISK theory is advanced to explain the origin of TIS.

The Ekman-wave-CISK is a low-frequency instability with a typical growth rate on an order of 10^{-6} s^{-1}. The unstable mode has a multi-scale wave packet structure: Global-scale circulation couples with a large-scale (several thousand km) precipitation complex. The latter in turn consists of a few synoptic-scale (one thousand km) precipitation cells that are accompanied by boundary-layer equatorial westerly surges. The wave packet moves eastward with a group speed slower than the phase speed of individual cells. The theory provides new physical insights into some observed key features of TIS, such as their low-frequency development/decay, multi-scale structure, slow eastward movement, longitude-dependent life cycle, and seasonality.

1. Introduction

The variability of the tropical atmospheric circulation has a remarkable low-frequency component characterized by the 40-50 day oscillation discovered by Madden and Julian (1971, 1972) (hereafter referred to as Madden-Julian Oscillation or MJO). This oscillation is a relatively broad-band phenomenon, thus also referred to as 30-60 day or intraseasonal oscillation in the literature. It has a characteristic frequency scale (defined by the inverse of a quarter period) of 10^{-6} s^{-1}, which is in between synoptic-scale (10^{-5} s^{-1}) variation and annual cycle (10^{-7} s^{-1}).

In the past two decades or so, especially since 1980's, a large number of studies using various atmospheric variables have established a firm observational foundation for tropical intraseasonal variations. A considerable body of theoretical and modeling work aimed at explanation of MJO have emerged since mid-1980's. Discussion in this paper focuses on theoretical aspects of MJO. It begins with a

Corresponding author address: Bin Wang,Department of Meteorology,2525 Correa Road,Honolulu,HI 96822,USA

*School of Ocean and Earth Science and Technology Publication Number 3137

concise description of observed features of MJO. Those features are, judged by the author, most relevant to the understanding of the phenomenon. They are also used to verify theories. Section 3 reviews current theoretical hypotheses on the nature of MJO. In the interest of brevity, no attempt is made to trace back the complete history of the theoretical development or to summarize all current theoretical and modeling research results. Instead, a unified theoretical model is proposed in section 4 to examine the major hypotheses pertaining to the basic dynamics of TIS. In particular, an Ekman-wave-CISK theory is presented in section 5 to account for the origin of TIS. The last section discusses the relevance and limitations of the current theories in interpreting MJO and presents some outstanding issues that call for future investigations.

2. Observational background

Based on the analysis of Canton rawinsondes, Madden and Julian (1971) revealed coherent structures among surface pressure, lower and upper troposphere zonal wind, and tropospheric temperature over a broad time scale that maximized between 41 to 53 days. In a subsequent paper, Madden and Julian (1972) examined data from other stations and found a significant coherence in the 40-50 day range among stations far removed from each other. As a summary, Madden and Julian suggested that the 40-50 day oscillation was the result of an eastward movement of large-scale circulation cells oriented in the tropospheric equatorial plane as illustrated schematically in Fig. 1.

After Madden and Julian's pioneering works various aspects of the oscillation have been intensively investigated in terms of velocity potential and winds (e.g., Lorenc 1984; Krishnamurti et al. 1985; Knutson

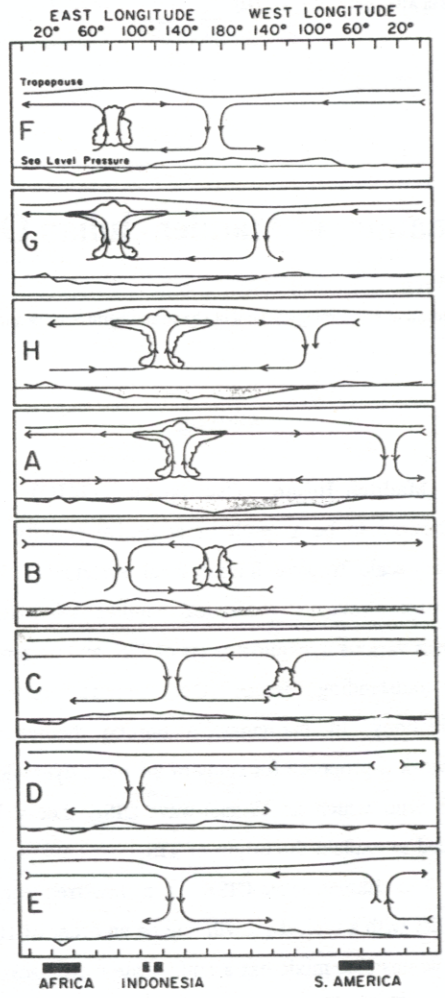

Fig. 1 Schematic depiction of the time and space (zonal plane) variations of the disturbance associated with Madden-Julian oscillation. Symbolic dates shown at the left of each chart correspond to dates associated with the oscillation in Canton's station pressure. The mean pressure disturbance is plotted at the bottom of each chart. The circulation cells are based on the mean zonal wind disturbance. Regions of enhanced large-scale convection are indicated schematically by the cumulus and cumulonimbus clouds. Taken from Madden and Julian (1972).

et al. 1986, Knutson and Weickmann 1987), OLR (e.g., Lau and Chan 1983, 1985, 1986a; Weickmann et al. 1985; Murakami et al. 1986; Nakazawa 1988, Wang and Rui 1990a), and atmospheric angular momentum (e.g., Anderson and Rosen 1983). These studies revealed many new features of the oscillation. For current knowledge of the observational aspects of the oscillation, readers are referred to a forthcoming comprehensive review by Madden and Julian (In preparation for Monthly Weather Review).

Madden and Julian's (1972) suggestion forms a plausible working hypothesis: the oscillation results from collective activity of a large number of low-frequency (intraseasonal) convection/circulation systems. From both a theoretical and a practical point of view, it is more meaningful to identify and analyze those intraseasonal disturbances. Individual cases were described in the literature by Krishnamurti et al. (1985) and Weickmann and Khalsa (1990) using 5-day or 3-day mean wind, pressure, and OLR data. Using pentad-mean anomaly maps of OLR, Wang and Rui (1990a) defined objectively intraseasonal convection anomalies and studied their development and movement. Rui and Wang (1990) further used ECMWF (European Centre for Medium-range Weather Forecast) analyzed winds and derived a composite circulation anomaly associated with six strongest cases. The coherency between OLR and circulation anomalies suggests that the convection/circulation anomalies as seen from the pentad-mean anomaly maps should be regarded as coherent dynamic systems. They are termed in this paper as Tropical Intraseasonal Systems (TIS). In the remaining part of this section the observed features of TIS that are believed to be most relevant to the understanding of the dynamics of MJO are summarized.

a. Vertical and horizontal structure

Madden and Julian (1971) found that the surface pressure anomaly is in phase with the 850 hPa zonal wind (surface low-pressure anomaly is accompanied by low-level easterly anomaly), out of phase with the upper-troposphere (300 to 100 hPa) zonal wind anomaly, and nearly in phase with temperature anomalies from 700 to 150 hPa. This finding indicates that the vertical structure of TIS, similar to those of the time-mean circulation and synoptic-scale disturbances, is dominated by the gravest baroclinic mode. In the boundary layer, the equatorial westerly surges tend to accompany convection (Lau et al. 1989).

The horizontal structure of TIS appears to be characterized by a coupling between Kelvin wave and the Rossby wave with the lowest meridional index. Using composite near-equatorial station data, Madden (1986) showed that eastward-moving convection anomalies force a Kelvin-like wave to the east and anticyclonic Rossby-like waves to the west with dominant anticyclonic eddies occurring in the summer hemisphere. Knutson and Weickmann's (1987) empirical orthogonal function (EOF) analysis of National Meteorological Center (NMC) wind and OLR data revealed that anomalous upper tropospheric cyclones are located to the east of the convection and anticyclones alongside or west of the convection with prominent rotational flow patterns in the winter hemisphere. By compositing the six strongest eastward-moving TISs, Rui and Wang (1990) found that the convection is nearly in phase with 200 (850) hPa equatorial easterlies (westerlies). The equatorial

easterlies (westerlies) are, in turn, coupled with twin anticyclones (cyclones) residing on each side of the equator. This composite structure shares similarities with the EOF patterns of Knutson and Weickmann (1987) and Murakami (1988).

b. Movement

The movement observed from pentad-mean anomaly maps of OLR is more complex than those documented by EOF or correlation-map analyses. Wang and Rui (1990a) found 122 TISs during a ten-year period (1975-1985 with 1978 missing). Of those 64% were dominantly eastward, 22% were independent northward, and 14% were westward propagation.

The eastward-moving TIS have, on average, strongest intensity and take three major paths as depicted in Fig. 2: (1) along the equator from Africa all the way to the mid-Pacific, (2) initially eastward along the equator, then turning at 100°E either toward the northwest Pacific monsoon trough in boreal summer or toward the South Pacific convergence zone (SPCZ) in austral summer, and (3) eastward along the equator with splitting center(s) moving northward over the tropical Indian or western Pacific Oceans or both.

Yasunari (1979, 1980) first related eastward-propagating near-equatorial MJO to the active/break periods of Indian summer monsoon. The northward propagation of cloud bands with a typical speed of about one degree latitude per day is connected with equatorial MJO. This type of northward propagation is similar to the path shown in Fig. 2c. It should be emphasized, however, that about one-half of the northward-propagating TIS are independent of equatorial eastward-moving TIS. They occur either in the Indian or in the western Pacific summer monsoon

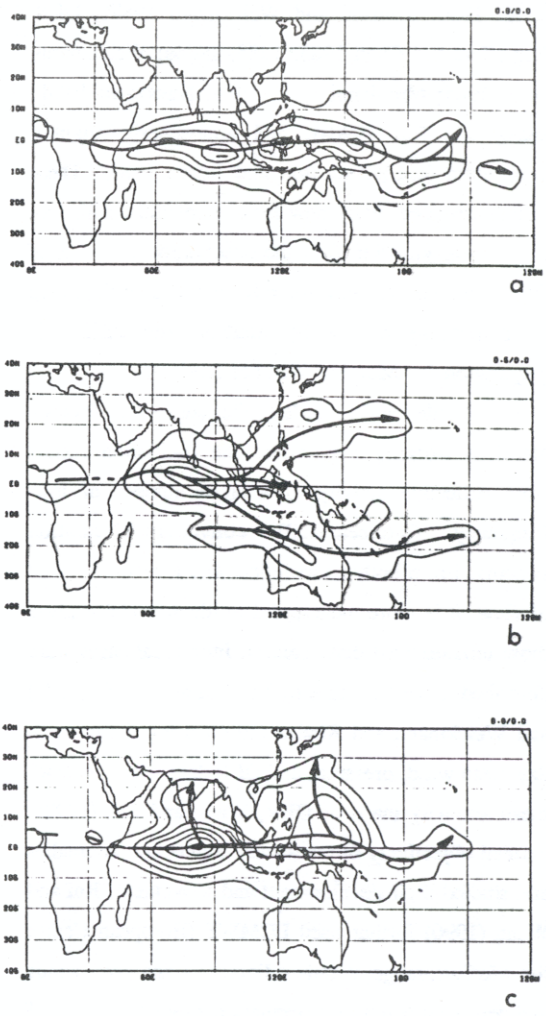

Fig. 2 Contour plot of the total number of occurrences of intraseasonal OLR anomalies that move eastward along the equator (a), move eastward and then turn either northeastward or southeastward around 100°E (b), and move eastward with splitting centers moving northward in the Indian and western Pacific monsoon domains (c), in each 2x2° box for a 10-year period (1975-1978 with 1978 missing). Contour interval is 0.8 in (a) and (c), and 0.6 in (b). The heavy lines indicate the central paths. Adopted from Wang and Rui (1990a).

domain. The meridional propagation in the western Pacific was documented by Chen and Murakami (1988).

The westward-moving systems have smaller spatial scales and much weaker intensities than the eastward-moving TIS. They are observed primarily about one Rossby radius of deformation (10-15° latitude) away from the equator and in the summer hemisphere. Cadet (1983), Murakami (1984) and Nakazawa (1988) also found westward propagating cloud anomalies, mostly west of 140°E. The westward-moving TIS appears to resemble Rossby waves modified by convective heating.

Knutson and Weickmann (1987) noticed longitudinal variations in movement. In the eastern hemisphere the upper and lower troposphere circulation anomalies couple with convection and move eastward slowly at a speed of about 5 ms^{-1}, whereas in the western hemisphere only upper tropospheric circulation anomalies are evident which travel at a speed about three times faster after they decouple from convection anomalies.

c. Development and life-cycle of the eastward-moving TIS

Knutson and Weickmann (1987) first produced a life-cycle of MJO mode based on a 6-year composite EOF analysis. On the basis of composition of 36 individual eastward-moving TIS, Rui and Wang (1990) proposed a four-stage life cycle: Initiation over the equatorial Africa; rapid development as passing through the equatorial Indian Ocean; mature evolution characterized by an intermittent weakening over the Indonesian archipelago and re-intensification over the western Pacific warm pool; and final decay near the dateline or emanation from the equatorial central Pacific toward subtropical North America and southeastern Pacific. The emanation from east of the dateline to North America confirms the findings of Lau and Phillips (1986).

The maximum intensification rate as measured by OLR anomalies are in the central equatorial Indian Ocean with secondary preferred areas of intensification in the northwestern Pacific monsoon trough during boreal summer and extending from northern Australia to the dateline south of the equator during austral summer (Wang and Rui 1990a). The maritime continent and central Pacific are regions of decay.

d. Multi-scale characteristics

Whereas circulation anomaly exhibits a global zonal scale (wavenumber one), the precipitation (OLR) anomaly of TIS is concentrated in an area with a zonal scale of a few thousand kilometers. The updraft branch in the precipitation (wet) region is much more intense than its downdraft counterparts in the surrounding dry areas. Within the wet region, the cloud mass exhibits a multi-cell structure. Nakazawa (1988) found that the OLR anomalies of MJO mode were often composed of a few eastward-moving super cloud clusters (SCC) which have a horizontal scale of one thousand kilometers. Each SCC in turn consists of several westward-propagating smaller cloud clusters (CC) which have an individual life span of 1-2 days and a scale of one hundred kilometers (Fig. 3). The eastward movement of SCC is in a discrete manner due to the successive formation of a new CC which propagates westward and becomes either damped or moves away from the equatorial regions.

e. Seasonality

The activity of MJO is evidently of season

dependence. Although it occurs throughout the annual cycle without a systematic change in periodicity (Anderson et al. 1984), the locations of maximum OLR variability and its extratropical response do exhibit seasonality (Knutson and Weickmann, 1987). Madden (1986) showed that the zonal wind anomaly in the 40-50 day time-scale exceeds that in adjacent lower and higher frequency bands by the largest amount during December through February. Similar conclusions were reached by Gutzler and Madden (1989). Wang and Rui (1990a) found that the eastward-moving TIS not only occurs more frequently but also has a larger amplitude from November through April, whereas the independent northward- and westward-moving TISs occur predominantly in boreal summer from May to October.

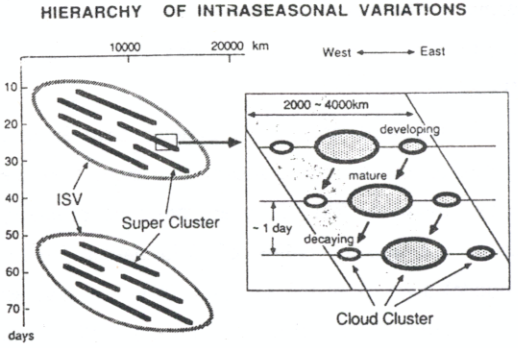

Fig. 3 Schematic description of the hierarchy of Madden-Julian oscillation mode. The left chart shows intraseasonal variation (ISV) consisting of groups of SCC moving eastward. The right chart illustrates the fine structure of the SCC which was composed of smaller-scale CCs moving westward, developing and decaying in one to two days. Adopted from Nakazawa (1988).

3. Theoretical hypotheses

Understanding of the physical processes that govern the development, propagation, spatial structures, and seasonality of TIS has been a primary objective of recent theoretical studies.

Many essential features of MJO are reproducible in various versions of atmospheric general circulation models (GCMs). The success of an aqua-planet GCM (Hayashi and Sumi 1986) and GCMs with axially symmetric climatology (Lau and Lau 1986; Hayashi and Golder 1986) in simulating MJO indicates that neither land-sea thermal contrasts nor zonal asymmetry is necessary to explain the existence of the oscillation (Emanuel 1987). The numerical simulations demonstrated that the model counterparts of MJO are caused by eastward movements of planetary-scale circulation systems which emplace their maxima near the equator and penetrate the entire troposphere with a baroclinic structure. Their horizontal structure resemble either a Kelvin wave (Swinbank et al. 1988; Lau et al. 1988) or a coupled Kelvin-Rossby mode (Hayashi and Sumi 1986; Hendon 1988; Hayashi and Golder 1988). These results strongly support the present working hypothesis. The aforementioned numerical studies also suggest that the condensational heating interacting with dynamic processes is responsible for the generation and maintenance of these long-lasting planetary scale modes.

On the basis of a scale analysis, Wang (1988a) argued that the principal energy source that maintains TIS must come from condensasional heating. The intraseasonal variation in precipitation rate over the Indian and western Pacific is about 3 mm day^{-1}. The heating rate due to this precipitation rate is shown to force a divergence motion of O (5×10^{-7} s^{-1}) that is necessary and sufficient to maintain the vorticity

balance and the baroclinic structure of TIS. This inference appears to agree with the observational diagnoses of Murakami et al. (1984) and Krishnamurti et al. (1985). They concluded that over the Indian and western Pacific Oceans the divergent wave associated with MJO is thermally direct with a net conversion of eddy available potential energy from diabatic heating over this frequency range. In the eastern Pacific, however, the intraseasonal variability is possibly forced by high-frequency eddy kinetic energy conversion (Murakami and Nakazawa 1985).

The dynamic processes of MJO must invoke some fundamental modes in the tropical atmosphere. The observed TIS has a zonal scale of globe and a meridional scale of the equatorial Rossby radius of deformation. This anisotropic scale yields a semi-geostrophic nature of TIS. It implies that the equatorial Kelvin and long Rossby waves are probably the most relevant modes, among others, to the dynamics of TIS.

There have been two different standpoints regarding how diabatic heating generates TIS. The first regards TIS as a manifestation of the atmospheric response to an imposed stationary heat source pulsating in intensity with a period of 40-50 days (Yamagata and Hayashi 1984; Anderson and Stevens 1987a) or a moving heat source with either constant strength (Chao 1987) or oscillatory strength (Hayashi and Miyahara 1987). The models taking this point of view are extensions of Gill (1980) model with heat sources pulsating in intensity or moving eastward. An obvious weakness with this type of model is the absence of feedback of atmospheric motion to heat source without which the development and movement (or selection of frequency scale) cannot be explained. The other viewpoint contemplates a more realistic heating interacting with circulation. The interaction between large-scale circulation and organized moist convection plays an essential role in the generation and maintenance of disturbances. Three hypotheses have been proposed and tested in terms of prototype of linear models.

The first follows wave-CISK (conditional instability of the second kind) thinking (Hayashi 1970; Lindzen 1974) and emphasizes the interaction between equatorial Kelvin wave-induced moisture convergence and convective heating (Chang 1977; Lau and Peng 1987; Chang and Lim 1988). Although the Kelvin wave-CISK mechanism can be responsible for slow eastward propagation, it does not explain the preferred large-scale instability.

The second hypothesis considers the interaction between surface evaporation and wind. The evaporation-wind feedback mechanism was shown to be important to the MJO in an idealized GCM model, but the existence of the model oscillation does not depend on it (Neelin et al. 1987). The model of Emanuel (1987) presumed an easterly basic flow and a neutrally stratified atmosphere (which deliberately excludes wave-CISK). The east-west asymmetries in perturbation latent heat fluxes leads to an eastward phase propagation and amplification. Similar to the wave-CISK, the evaporation-wind feedback makes perturbations grow unboundedly with decreasing wavelength. In addition, the observed climatological low-level winds over the equatorial eastern hemisphere where the oscillation is strong are either weak westerlies or quiescent (Wang 1988b). This jeopardizes the application of the linear wind-evaporation feedback model to real atmosphere.

The last hypothesis invoked a feedback between

the boundary layer friction-induced moisture convergence and precipitational heating (Wang 1988a). Since the Ekman pumping-induced moisture convergence is not in phase with the wave-induced moisture convergence, the heating due to boundary-layer moisture convergence results in an instability favorable for planetary scales (Wang and Chen 1989). This mechanism will be referred to as Ekman convergence-precipitation heating (EC-PH) feedback.

The interaction between convective heating and circulation is inherently nonlinear even for small-amplitude disturbances (Lim et al. 1990). The multi-scale, asymmetric wet-dry structure of TIS can not be described by linear wave-like normal mode. Examination of the three hypotheses in a dynamic framework which contains nonlinear (also referred to as conditional or positive-only) heating is necessary.

Nonlinear wave-CISK heating was shown to be able to produce an exponentially growing wavenumber-one flow pattern that travels eastward without change of shape (Lau and Peng 1987). As the model resolution increases, however, the precipitation region of the fast-growing mode displays decreasing scales (Lim et al. 1990). Itoh (1989) also found that high-wavenumber disturbances could be favored, and in order for a SCC dominates among many possible growing CCs he had to artificially suppress the generation of convection by weak moisture convergence over wide areas of dry regions. Using analytical models of wave-CISK, Dunkerton and Crum (1991) and Wang and Xue (1992) have shown that the nonlinear wave-CISK heating favors a narrow precipitation region and yet remains global in the circulation extent, but the growth rate is inversely proportional to the width of the wet region. In this sense, the nonlinear wave-CISK, similar to linear wave-CISK, favors the smallest scales. Failure to select a finite scale remains a disturbing property of the nonlinear wave-CISK.

In the next section a unified theoretical framework which includes all three mechanisms will be introduced. With this model the instability induced by EC-PH feedback (Ekman-wave-CISK) will be examined.

4. A unified basic theoretical framework: Two and one-half layer model

This model is designed to contain only essential physics which are sufficient for simulating fundamental features of TIS discussed in section 2. To focus on EC-PH feedback mechanism, the model neglects advective nonlinearity and includes only the nonlinearity associated with heating that acts even for small-amplitude perturbations. The model is a nonlinear extension of Wang and Rui's (1990a) model and a simplified version of the model described by Wang and Li (1992). For this reason the description of the equations of motion is brief.

The present model consists of a two-layer free troposphere and a boundary layer, describing three vertical modes: Baroclinic and barotropic modes of the free troposphere and a boundary layer mode. The precipitational heating released in the middle troposphere stimulates only the baroclinic mode. If the vertically integrated divergence in the free troposphere vanishes the barotropic and baroclinic modes are decoupled even in the presence of boundary layer. It has been demonstrated that the variations associated with the barotropic mode are an order of magnitude smaller than that with the baroclinic mode in the tropics (Wang and Rui 1990b; Wang and Li 1992). A

fundamental approximation is made here to remove the free troposphere barotropic mode, so that the model is composed of a free-troposphere baroclinic mode and a boundary-layer mode. In this sense, the present model may be referred to as a two and one-half layer model. The dimensional governing equations on an equatorial β-plane are

$$\partial u/\partial t - \beta yv = -\partial\phi/\partial x + r\nabla^2 u, \quad (1a)$$

$$\partial v/\partial t + \beta yu = -\partial\phi/\partial y + r\nabla^2 v, \quad (1b)$$

$$\partial\phi/\partial t + C_0^2(1-\delta I)\nabla\cdot\mathbf{V} = C_0^2 d(\delta B-1)\nabla\cdot\mathbf{V}_B - \delta F|\mathbf{V}_B|(q_s-q_0), \quad (1c)$$

$$E_1 u_B + \beta y v_B = -\partial\phi/\partial x, \quad (1d)$$

$$E_2 v_B + \beta y u_B = -\partial\phi/\partial y, \quad (1e)$$

where $\mathbf{V}$ (u, v) and $\mathbf{V}_B$ (u_B, v_B) are the lower-troposphere and boundary-layer winds, respectively; ϕ the lower-troposphere geopotential; r is horizontal momentum diffusion coefficient (10^6 m^2s^{-1}), C_0=50 ms^{-1} denotes the dry gravity wave speed of the free-troposphere baroclinic mode.

In the thermodynamic equation (1c) the nondimensional parameter δ is a heating switch-on function. Here it is simply assumed that δ=1 if the precipitation rate is positive, i.e., $-C_0^2(I\nabla\cdot\mathbf{V}+dB\nabla\cdot\mathbf{V}_B)+F|\mathbf{V}_B|(q_s-q_0) > 0$, and δ=0 otherwise. Four nondimensional parameters in (1c) are defined as follows

$$I = RL_c b(q_3-q_1)/(C_p p_2 S_2 \Delta p)$$ The heating coefficient in the free troposphere, (2a)

$$B = RL_c bq_c/(C_p p_2 S_2 \Delta p)$$ The heating coefficient in the boundary layer, (2b)

$$F = RL_c b\rho_s g C_D/(2C_p p_2)$$ The evaporation coefficient, (2c)

$$d = (p_s-p_c)/\Delta p$$ The depth of the boundary layer, (2d)

where R, g, L_c, C_p, p_2, p_s, p_c, ρ_s and C_D are the gas constant for dry air, the gravity, the latent heat of condensation, the specific heat at constant pressure, the pressure at the middle free-troposphere, the surface pressure (1000 hPa), the pressure at the top of the boundary layer, the air density at the surface, and the drag coefficient (1.5×10^{-3}), respectively; b is a precipitation efficiency coefficient measuring the fraction of total moisture convergence which condenses out as precipitation; q_c, q_3, and q_1 are vertical mean specific humidity in the boundary layer, the lower and upper free-troposphere, respectively. Here q_1 is taken as a constant (0.0004), q_c and q_3 are given by

$$q_c = q_0(p_s^m-p_c^m)/m(p_s-p_c), \quad (3a)$$

$$q_3 = q_0(p_c^m-p_2^m)/m(p_c-p_2), \quad (3b)$$

where pressure p_s, p_c, and p_2 have been divided by 1000 hPa; and $m=H/H_1$ with H=7.6 km being the density scale height and H_1=2.2 km being the water vapor density scale height. In derivation of (3a,b) it was assumed that the absolute humidity of the basic-state atmosphere falls off with height exponentially with a constant water vapor density scale height H_1 (Wang 1988a). The surface air specific humidity q_0 is assumed to be a function of SST (in units of °C) given by the following empirical regression equation (Li and Wang 1992):

$$q_0 = (0.972\ SST - 8.92)\times10^{-3}. \quad (4)$$

The q_s in (1c) is the specific humidity at the SST which can be calculated from the Clausius-Clapyron equation.

The Rayleigh friction coefficient in the boundary

layer can be expressed as a function of surface roughness (z_0=0.01 m), surface-layer depth (h=40 m), the pressure depth of the boundary layer, and the turbulent viscosity (A_z=10 m^2s^{-1}), namely

$$E = \rho_s g A_z/[h(p_s-p_e)\ln(h/z_0)], \quad (5)$$

In the standard run, we set E_1=E and E_2=2E to mimic the observed feature that was derived based on diagnosis of climatological monthly mean data (Li and Wang 1992).

Equation (3) indicates that the vertical distribution of the moisture content hence the moist static energy depends on SST; therefore the heating coefficients I and B are also controlled by SST. From the thermodynamic equation (1c), one can readily identify three mechanisms as three key parameters: wave-CISK represented by parameter I, evaporation-wind feedback denoted by parameter F, and EC-PH feedback represented by parameter B.

Equations are solved in an equatorial beta-plane channel. The solutions are periodic in zonal direction, and the north and south boundaries are open. Boundary conditions on the open boundaries require the partial derivatives normal to the boundary vanishing. These conditions ensure that there is no diffusion of mass, momentum, and temperature across the boundaries.

The finite-difference method in both space and time is adopted. The time interval is set 30 minutes and the spatial resolution is 5° longitude by 2° latitude. In addition to central-difference time-integrating scheme, Euler forward and backward methods are used every 12 hours to reduce noise. Initially, an equatorially trapped easterly Kelvin wave perturbation is centered at the equator and 40°E with a zonal scale of 4000 km and a cosine structure. Time integration was then carried out for 40 days to obtain temporal evolution of the perturbation. The growth or decay of the moist unstable mode is measured by its maximum precipitation rate which indicates the maximum generation rate of the total (available potential plus kinetic) energy of the unstable mode. The growth rate determined in this manner is consistent with those derived from kinetic or available potential energy. For the standard run, the following parameters are used: p_e=900 hPa, Δp=400 hPa, SST = 29°C, b=0.9, so that I=0.84 and B=1.73.

5. Ekman-wave-CISK

a. Instability regime

In the present two and one-half layer model, the heating due to the moisture convergence of the free-troposphere wave motion (hereafter referred to as wave-convergence heating) reduces static stability S_2 to an effective static stability, $(1-I)S_2$, in the heating region and generates eddy available potential energy. The intensity of the wave-convergence heating (parameter I) and associated moist gravity wave speed $(1-I)C_0$ depend on the moisture content in the lower free troposphere which increases with increasing SST and decreases with deepening boundary layer (Fig 4). When parameter I exceeds the unit, the moist gravity wave speed reduced to zero and the atmosphere falls in an unstable wave-CISK regime (Fig. 4a). In that case, the wave-convergence heating-induced eddy available potential energy exceeds the amount of energy converted to eddy kinetic energy, so that a thermally direct instability occurs, leading to an unbounded growth for infinitesimal scales.

The presence of a boundary layer, however, reduces the wave-convergence heating, making the atmosphere stable to wave-CISK (I < 1). This implies

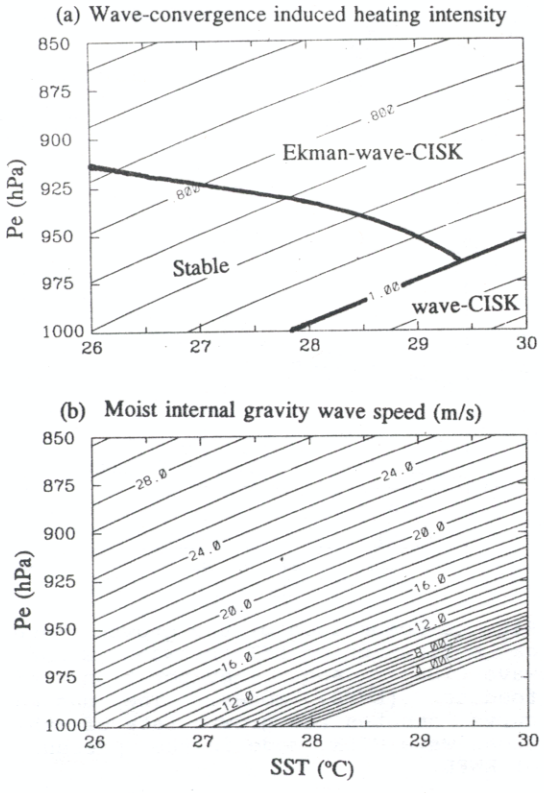

Fig. 4 Dependence of (a) wave convergence-induced heating intensity and (b) corresponding moist internal gravity wave speed on sea surface temperature and the depth of the boundary layer as measured by the pressure at the top of the boundary layer p_t. The marginal Ekman-wave-CISK curve is based on the growth rate computed for the first 10 days of integration.

that the presence of a boundary layer can effectively remove the catastrophe of the wave-CISK. On the other hand, in this stable wave-CISK regime, perturbations can become unstable owing to the additional heating provided by the boundary-layer moisture convergence (hereafter referred to as Ekman-convergence heating). The instability due to the EC-PH feedback mechanism is referred to as Ekman-wave-CISK regime (Fig. 4a).

b. Low-frequency instability

To identify the effect of EC-PH feedback, the surface evaporation term was excluded by setting F=0 in (1c). Under a uniform SST=29°C, when the top of the boundary layer is higher than 980 hPa the wave-convergence heating coefficient I is less than unit (Fig. 4a). The Ekman-convergence heating, however, destabilizes the atmosphere and may result in growing mode. For a shallow boundary layer (p_e=950 hPa) the initial perturbation decays slowly with an exponential decay rate of about 0.03 day^{-1} due to insufficient destabilization effect of the boundary layer (Fig. 5). When the depth of the boundary layer increases, although the wave-convergence heating weakens and the moist free troposphere is effectively stabilized, the increasing Ekman-convergence heating overcomes the wave-CISK stabilization, causing amplification of disturbances. The transition from an oscillatory decay to an oscillatory growth occurs when the top of the boundary layer rises from p_e=940 to p_e=930 hPa. As the boundary layer further deepens (p_e=920 hPa) the amplitude increases exponentially with a growth rate of 0.06 day^{-1}.

The unstable mode destabilized by the EC-PH feedback grows or decays slowly. The growth rate increases with increasing SST and boundary layer depth (figure not shown). For a fixed boundary layer depth (925 hPa for example), a critical SST (27.5°C) is required in order for a perturbation to grow. For a wide range of SST (from 25 to 30°C) and boundary layer depth (p_e from 950 to 825 hPa), the growth rate varies from -0.05 to 0.2 day^{-1}, which is of O (10^{-6} s^{-1}),

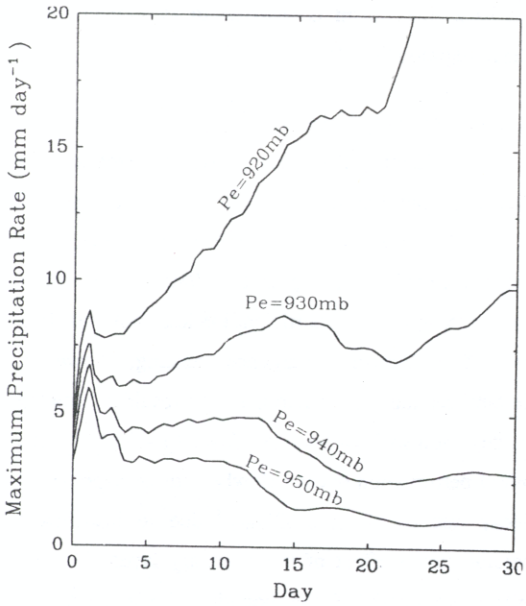

Fig. 5 The maximum precipitation rate of the Ekman-wave-CISK modes as a function of time for different boundary layer depths.

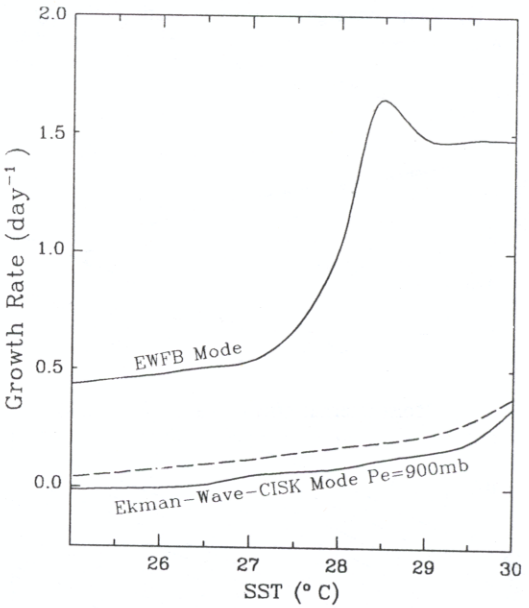

Fig. 6 Comparison of the growth rate as a function of SST between Ekman-wave-CISK and evaporation-wind feedback (EWFB) modes. The dashed curve denotes the growth rate of the Ekman-wave-CISK mode in the presence of EWFB.

an order of magnitude smaller than the typical growth rate of synoptic-scale disturbances. This low-frequency instability appears to cope with the observed growth rate estimated from OLR field by Wang and Rui (1990a).

In the stable wave-CISK regime, the evaporation-wind feedback can also lead to exponentially growing modes (Xie et al., personal communication); however, in the absence of planetary boundary layer the evaporation-wind feedback mechanism causes a synoptic-scale fast growth with a typical growth rate of O ($10^{-5}s^{-1}$) as shown in Fig. 6. In the comparison all model parameters are identical except in one case F=0 (no evaporation) and p_e=900 hPa whereas in the other p_e=1000 hPa (no boundary layer) but evaporation heating term is retained. Note that when SST is higher than 28°C the unstable evaporation-wind feedback mode merges into an unstable wave-CISK mode.

When both the EC-PH and evaporation-wind feedbacks are included, the growth rate of the unstable mode is close to that of the Ekman-wave-CISK mode (Fig. 6). This indicates the dominance of the effect of boundary-layer moisture convergence over the evaporation effect. The low-frequency instability of the Ekman-wave-CISK mode does not change qualitatively in the presence of evaporation-wind feedback. On the other hand, without boundary layer process the evaporation-wind feedback leads to a fast synoptic-scale growth.

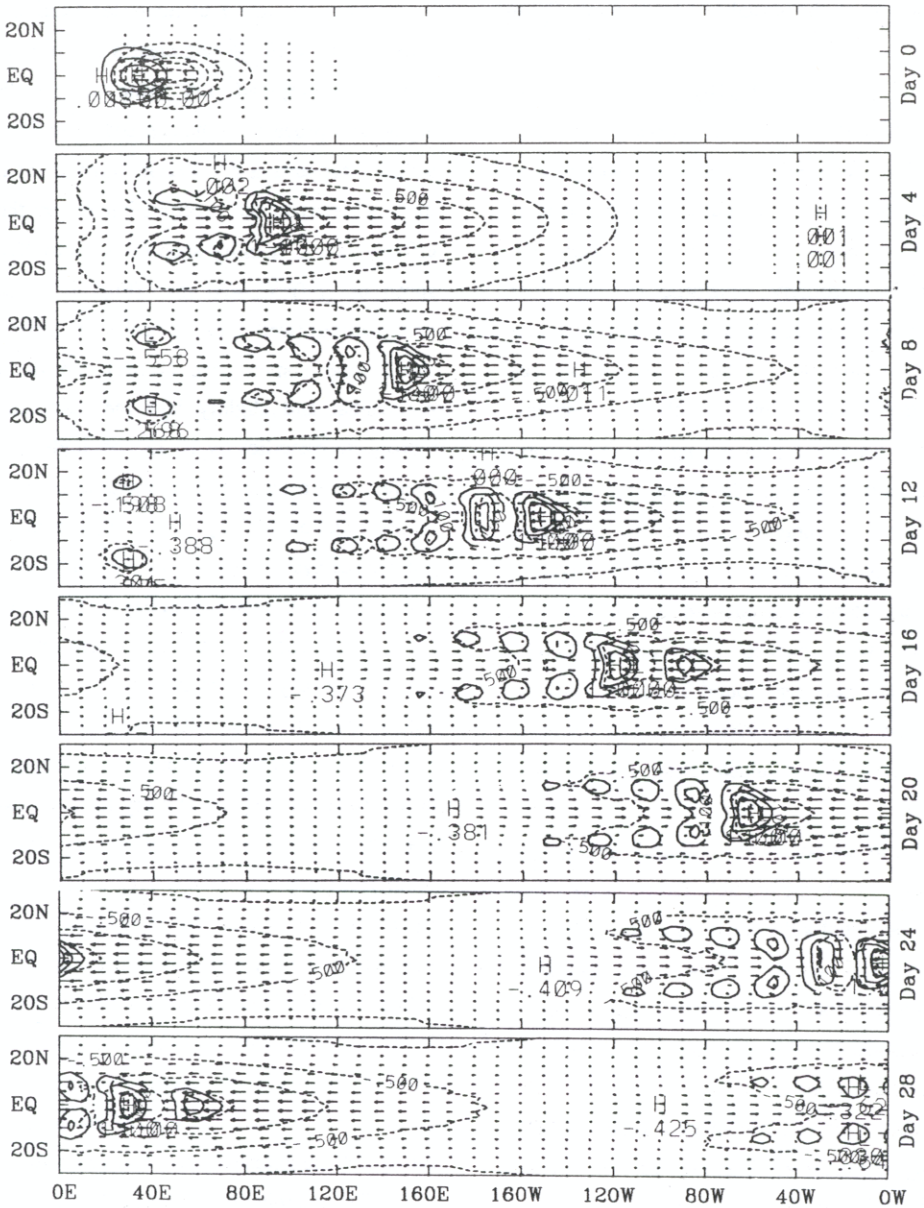

Fig. 7 Sequential maps of precipitation rate (solid contours) and lower troposphere geopotential (dashed contours) and winds (arrows) for the standard run at interval of 4 days. All three fields are normalized by their corresponding maximum amplitudes at each panel. The contour starts from 0.1 at an interval of 0.2.

c. The structure of the unstable Ekman-wave CISK mode

Figure 7 depicts temporal evolution of the precipitation rate and lower-troposphere geopotential and wind fields. There is an initial adjustment process during which the horizonal structure and zonal scale of the initial perturbation evolve rapidly. Initially, the perturbation is a solitary equatorial easterly (low pressure) Kelvin wave. The Ekman convergence in the boundary layer and precipitational heating induces substantial meridional inflow into the low pressure which excites westward propagating Rossby waves. The heating associated with the wave and boundary layer moisture convergence, however, integrates eastward-propagating Kelvin and westward-propagating Rossby waves, forming a coupled eastward-moving Kelvin-Rossby wave packet. The coupled Kelvin-Rossby wave structure was found in an earlier linear analysis (Wang and Rui 1990b), but the nonlinear unstable mode contains a much larger Rossby wave component.

Similar to the observed multi-scale structure of TIS (Nakazawa 1988), the unstable Ekman-wave CISK mode, after the initial adjustment, is characterized by three distinct zonal scales: a global-scale circulation system of wavenumber one; a large-scale (order of $5x10^3$ km) organized multi-cell precipitation complex, and synoptic-scale (order of 10^3 km) precipitation cells. The precipitation complex resembles a group of SCC described by Nakazawa. Because of the model resolution the CC-scale cells cannot be resolved.

The wavenumber-one circulation consists of a concentrated ascending (wet) region and two broader descending (dry) regions occuring on both sides of the wet region. This wet-dry asymmetry in zonal structure arises from the effect of nonlinear heating. Figure 8 illustrates how the heating creates a narrow moist core and a wide-spread dry zone during the initial adjustment process. In the descending region dry static stability supports a dry Kelvin wave speed of C_o=50 ms^{-1}, whereas in the precipitation region the reduced effective static stability supports a moist Kelvin wave speed of $(1-I)^{1/2}C_o$=20 ms^{-1} (Fig. 4b). The narrow precipitation (wet) area is nearly in phase with the zonal wind convergence ($\partial u/\partial x$) and the minimum geopotential and slightly lags the maximum lower troposphere easterlies by 10-15° longitude; they move together with a moist Kelvin wave speed. Outside of the precipitation region, on the other hand, the low geopotential system continuously expands until it fills in the entire equatorial belt at day 6. The east front of the easterlies propagates at a dry Kelvin wave speed of 50 ms^{-1} from day zero to day six, completing a total displacement of about 240° longitude. The Rossby waves (westerlies) were generated after about one day and thereafter propagated at a dry Rossby wave speed of about 17 ms^{-1} (about 1/3 of the dry Kelvin wave speed) from day one to day six, completing a total displacement of about 70° longitude. The energy dispersion in the dry region is finally restrained by the finite geometry of the full circumference of the globe. The formation of the wavenumber-one circulation is, therefore, a result of energy dispersion by dry equatorial waves that are excited by precipitational heating and the geometric restraint of Earth.

The precipitation complex displays a coupled Kelvin-Rossby wave packet structure. To the east of the central wave packet prevail strong equatorial easterlies and to the west are weaker westerlies, resembling a Kelvin wave. The cyclonic shears located

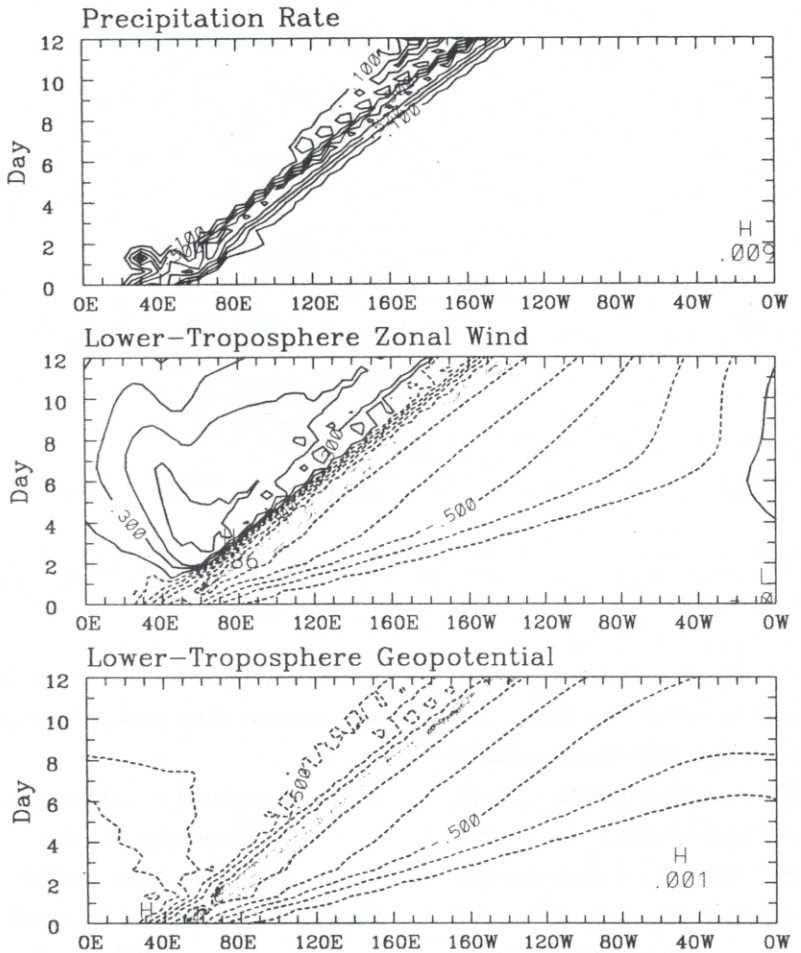

Fig. 8 Longitude-time diagram of precipitation rate and lower-troposphere geopotential and zonal wind along the equator for the standard run. As in Fig. 7 all fields are normalized. The contour interval is 0.2. The areas enclosed by contours of 0.9 (or -0.9) highlight moist core region.

on each side of the equatorial westerlies maintain positive relative vorticity cells that resemble Rossby wave trains. The precipitation complex consists of a few SCC's along the equator coinciding with the Kelvin wave low pressure and two off-equatorial trains of precipitation cells coping with the Rossby wave low pressures.

The precipitation cells within the wave packet are organized by the synoptic-scale boundary-layer moisture convergence. Figure 9 shows the relationship between the precipitation and the boundary layer winds, divergence, and vorticity. In contrast to the global scale of the lower free troposphere winds, the boundary layer winds have fine synoptic structures which match

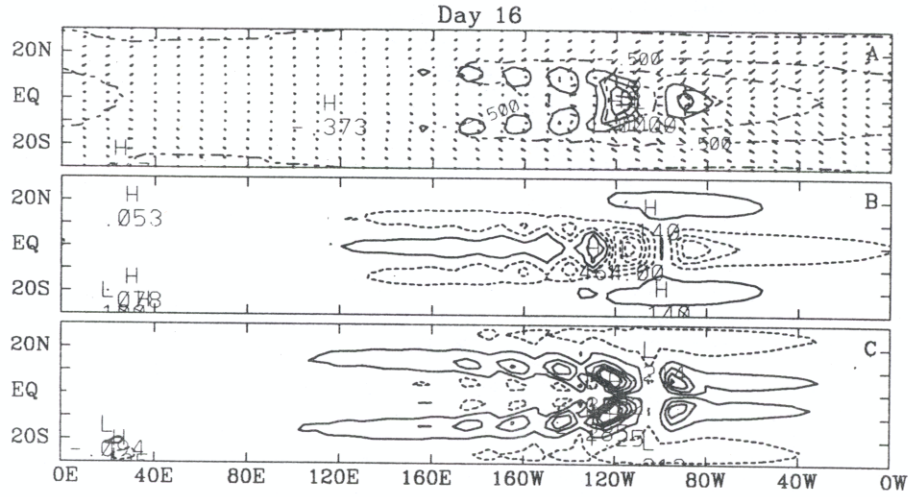

Fig. 9 (a) Precipitation rate (solid contours) and boundary layer wind, (b) boundary layer divergence, and (c) boundary layer vorticity for the standard run at day 16. Fields are normalized as in Fig.7.

precipitation cells extremely well. A notable feature is that equatorial westerly surges accompany each equatorial precipitation cell. Convergent meridional winds are connected to those westerly surges due to the beta-effect. This is a reminiscence of the observed westerly wind "burst" that often accompanies SCC occurring in the western Pacific. The off-equatorial precipitation cells are sustained by the Ekman convergence that is proportional to the cyclonic vorticity of Rossby waves. In fact, the solution of the boundary layer equations (1d,e) indicates that the boundary layer convergence comes from two principal tributes: near the equator the beta-convergence dominates, which generates convergence for equatorial westerlies, whereas away from the equator the Ekman convergence tends to be proportional to the vorticity at the top of the boundary layer (Lindzen and Nigam 1987; Wang and Chen 1989). It is the interaction between boundary-layer moisture convergence and precipitational heating that creates a coherent synoptic-scale structure of the individual precipitation cells.

d. The slow eastward movement of the wave packet

The precipitation complex of the unstable Ekman wave-CISK mode consists of dispersive precipitation cells. Figure 7 indicates that as a leading precipitation cell moves eastward (at day 4, for example), a new cell forms behind the leading cell (at day 8), rapidly develops (at day 12), and finally becomes the strongest cell (at day 16) and replaces the previous leading cell (at day 20). The dispersion process repeats itself from day 20 to day 32. As a result, the wave packet or energy propagates with a slower eastward group speed. The propagation speed of the maximum precipitation rate is the group speed of the wave packet. It is important to point out that the movement of low-geopotential center and the strongest easterly wind are both coupled with the movement of

the strongest precipitation cell, namely, the circulation and the precipitation complex moves together with the group speed of the unstable wave packet regardless of individual precipitation cells moving with a faster moist Kelvin wave speed. Figure 10 compares the group speed of the unstable wave packet with the phase speed of individual precipitation cells. The dispersion effect of the precipitation cells is more significant when the boundary layer becomes deep, indicating the critical role of boundary layer convergence in organizing these dispersive precipitation cells.

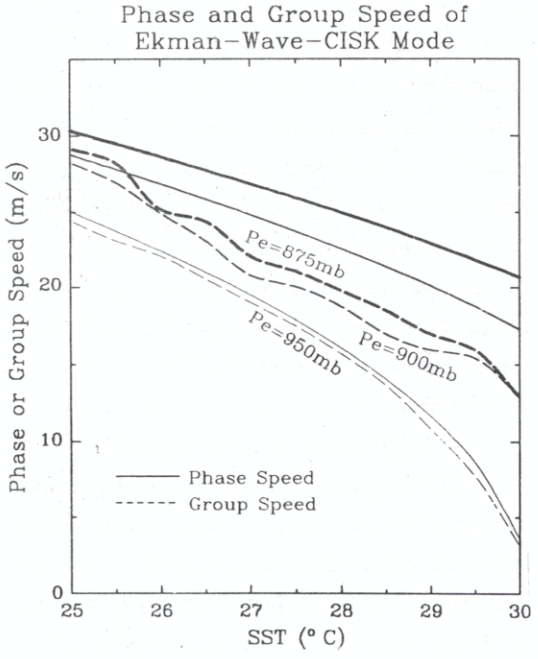

Fig. 10 Comparison of the group speed (solid) of the Ekman-wave-CISK mode with the phase speed (dashed) of the individual precipitation cells for different boundary layer depth. The thickest, medium, and thinnest lines correspond to p_t = 875, 900 and 950 hPa, respectively.

6. Summary and discussions

a. The basic dynamics of TIS

In this subsection, the results derived from theoretical models, especially from the Ekman-wave-CISK model, are verified against the observed features of TIS summarized in section 2. Most of these features are reproduced reasonably well by the models, and thus the mechanisms responsible for these features can be understood in terms of the model physics. Of course, cautions must be exercised in view of the limitations of the models.

1. The vertical and horizontal structure

Both the vertical and horizontal structures of the Ekman-wave CISK mode (Fig. 7) bear remarkable similarity to observed structures of TIS. The out-of-phase relationship between the upper and lower tropospheric winds results from the release of precipitational heating in the middle troposphere. The nearly in-phase relationship between low-level pressure and easterlies is a result of the balance between meridional pressure gradient force and the Coriolis force associated with zonal winds. The dominance of zonal winds near the equator with significant off-equatorial rotational wind component suggests that the observed TIS resembles a coupled Kelvin-Rossby wave packet. This structure was reproduced well, though in a somewhat idealized fashion, in the present Ekman Wave-CISK model as well as in many other simple nonlinear models (e.g., Hendon 1988). The process responsible for the coupling between equatorial Kelvin and Rossby waves in the present model is the precipitational heating induced by the boundary-layer moisture convergence, whereas is due to nonlinear advection in the Hendon's (1988) model.

2. The dominant slow eastward movement

With a uniform SST, the unstable mode in the present model travels eastward along the equator with a path similar to that shown in Fig. 2a over the eastern hemisphere. The dominant eastward propagation in the model is a result of the unstable mode selection. The Ekman convergence (along with higher SST near the equator in a more realistic SST distribution) favors the development of eastward-moving coupled Kelvin-Rossby mode. It was also suggested by Lau and Peng (1987) that nonlinear heating likely suppresses Rossby-wave response to the west and enhances Kelvin-wave response to the east of a propagating heat source. In Hendon's (1988) model, the unstable mode is able to stabilize the atmosphere through differential mean temperature advection, so that the zonal asymmetry in the static stability causes eastward propagation.

The slow propagation of the eastward-moving TIS is primarily due to precipitational heating. In the present model heating slows down eastward movement through reducing static stability and through coupling equatorial Kelvin and Rossby waves that generates dispersive precipitation cells, resulting in a slow group speed for the wave packet. In multi-vertical-mode models heating affects propagation in a similar way through reducing static stability (Swinbank et al. 1988; Lau et al. 1988). Slow propagation may also be caused by the coupling between different internal vertical modes (Chang and Lim 1988; Wang and Chen 1989), and by a heating profile with a maximum located in the lower troposphere (Takahashi 1987). Without convective heating, disturbances would move much faster as observed in the western hemisphere.

3. Development and life cycle

It has been shown that the low-frequency growth rate of the unstable mode increases with increasing SST for given boundary layer depth. The preferred development over the warm water of the Indian and western Pacific Oceans is a manifestation of favorable low-frequency instability of the moist tropical atmosphere to large-scale perturbations. This instability, depending on the vertical distribution of moist static energy of the basic flow, requires underlying SST exceeding a critical value. The disintegration of convection anomalies in the eastern-central Pacific results from the reduction in convective instability and moisture supply due to underlying cool ocean surface. The longitudinal variation of SST thus modulates convective activity and development, creating a sharp contrast in the strength of intraseasonal variations between the eastern and western hemispheres. The cause of the weakening over Indonesia archipelago, however, is not well perceived. A plausible hypothesis is that intense diurnal variation and synoptic-scale disturbances constantly tap moist static energy, effectively reducing the energy source available for the low-frequency development. The large surface friction over the islands may be another factor to weaken TIS.

4. Multi-scale wave packet structure

The multi-scale characteristics of the eastward travelling TIS, i.e., the global-scale circulation, the large-scale precipitation complex, and the synoptic-scale individual precipitation cell (SCC) as described by Nakazawa are captured by the Ekman-wave-CISK model. The wet-dry asymmetry, namely, the contrast between the global-scale circulation and the concentrated region of precipitation complex, is due to the effect of nonlinear heating. Nonlinear heating excites moist and dry equatorial waves in the wet and dry regions, respectively. The fast dry waves carry

energy away from the wet region and maintain the global scale of the disturbance. On the other hand, the heating in the wet region generates intense ascending motion which must be confined to a narrow zone in order to compensate the weak descending motion in much broader dry regions. The multi-cell precipitation complex is shown to be primarily organized by planetary boundary layer flows. This indicates the crucial role of the Ekman convergence-precipitation heating feedback in the maintenance of the multi-cell wave-packet structure of TIS.

5. Seasonality

The dependence of the instability and propagation speed on SST suggests that the annual march of SST could be one of the major climatic factors that are responsible for the observed annual variation of TIS. Wang and Rui's (1990b) linear instability analysis indicated that the growth rate of unstable waves decreases significantly when the maximum SST shifts from the equator (a boreal winter position) to 7.5°N (a boreal summer position). This explains why the strength of MJO is stronger in boreal winter than in boreal summer (Madden 1986). We have recently examined the response of the Ekman-wave-CISK mode to climatological January and July SST distributions. In January there is a marked southward shift of precipitation region toward northern Australia, inducing a monsoon depression-like Rossby wave train in Australian monsoon area. Conversely, in July there is a prominent northward or northwestward propagation of precipitation cells over the western Pacific, enhancing the summer monsoon trough in situ. Both the southward and northward propagation speeds are closely related to SST gradients. Those January and July tracks are reminiscences of the observed paths shown in Figs. 2b and c. In addition to the influence of SST, the effects of monsoon circulation and the Hadley cell may also play important roles in the seasonal variation of TIS as will be discussed in the next subsection.

b. Other dynamic aspects of TIS

In spite of the successes of simple theoretical models in interpreting some fundamental features of TIS, there remain many other important aspects of the oscillation which must be addressed by more sophisticated or specific models. Those aspects as well as some outstanding issues are discussed in this subsection.

1. The time-scale of the intraseasonal oscillation

It is generally recognized that the intraseasonal oscillation is a relatively broad-band phenomenon and is not present all the time. Based on OLR analysis of eastward propagating anomalies, Knutson et al. (1986) found a wide-spread period ranging from 20 to 79 days and the oscillation was present about 75% of time. Murakami (1987) pointed out that the eastward propagation of OLR anomalies was often interrupted by quiescent periods. These observations suggest that the averaged 40-50 day period should not be regarded as a highly tuned preferred periodicity. Under the working hypothesis that the oscillation is a result of collective activity of TIS, the broad-band periodicity and its irregularity and regional differences are naturally associated with the episodic development and, in particular, the slow movement of TISs. When prevailing eastward propagation is absent, the intraseasonal oscillation may be controlled by local instability, especially in the Indian and western Pacific Oceans, so that the period of the generation of

intraseasonal oscillation mode is possibly determined by other mechanisms such as convection-thermal relaxation feedback (Goswami and Shukla 1984), drying out-remoistening process or cyclic oscillations of the static stability (Hendon and Liebmann 1990; Hartmann et al. 1992).

2. Interaction between TIS and the mean basic flows

The time-mean circulation of the tropical atmosphere has considerable season-dependent zonal, meridional, and vertical variations. The effects of the basic flow on the evolution of TIS is an important issue. The structure and growth of various types of equatorial wave-CISK modes were shown to be very sensitive to the presence of the basic-state vertical shear (Zhang and Geller, personal communication). Lau and Peng's (1990) numerical experiment indicated that an equatorial Kelvin wave interacting with northern summer monsoon circulation may induce synoptic-scale baroclinic disturbances along 15-20°N. The simultaneous development of monsoon disturbances and weakening of the equatorial Kelvin wave result in a rapid northward shift of the rising branch of the local Hadley cell. Anderson and Stevens (1987b) showed that a zonally symmetric intraseasonal oscillation mode occurs when the basic state contains the advective effects of a divergent Hadley cell. Understanding of the interactions of TIS with mean flows is of central importance to the dynamics of monsoon and teleconnection.

3. TIS and high-frequency disturbances

The planetary-scale TIS modulates and interacts with high frequency disturbances. For instance, MJO appears to be phase-locked with 10-20 day medium-scale disturbances that travel westward (Krishnamurti et al. 1985). The contribution of organized storms and cyclones to the intraseasonal variability in the western Pacific-Indian Ocean region is substantial (Smith and Mehta 1990). The nature of the interactions among MJO and tropical cyclones, SCCs, and high-frequency cloud clusters is not well understood and requires further investigation.

4. TIS and monsoons

Tropical intraseasonal systems have profound influences on the onset, active/break, and retreat of Indian summer monsoon (Yasunari 1979; Sikka and Gadgil 1980; Krishnamurti and Subrahmanyam 1982; Murakami et al. 1986; Lau and Chan 1986a; Hartmann and Michelson 1989) as well as the Australian monsoon (Holland 1986; Hendon and Liebmann 1990). The existence of independent northward-moving disturbances (Wang and Rui 1990a) suggests that the mechanism responsible for the self-reliant northward propagation may differ from that of the equatorial eastward propagation. Slow northward propagation on a time-scale of 20-40 days was simulated in terms of zonally symmetric monsoon models (Webster 1983; Goswami and Shukla 1984; Gadgil and Srinivasa 1990; Srinivasan et al. 1991). Webster proposed that the surface latent and sensible heat fluxes into the boundary layer, which destabilizes the atmosphere ahead of the ascending zone, were the principal cause of the northward propagation. In addition, the influence of meridional SST gradients and mean monsoon circulation are also possible causes for the meridional penetration of TIS to monsoon domains.

Over the summer monsoon regions, MJO exhibits some characteristics of a stationary oscillation. Weickmann and Khalsa (1990) pointed out that there are two equatorial regions (100°E and 150°E) where

eastward-moving clouds experience a local intensification of convection. Zhu and Wang (1992) documented the out-of-phase pulsation of convection between the tropical Indian Ocean and western Pacific and termed it as 30-60 day convection seesaw. The seesaw occurring in boreal summer results from a time-lagged development of two transient TISs: The western system originates in the equatorial Indian Ocean and moves eastward and/or northward while the eastern system develops in the northwestern tropical Pacific and moves westward and/or northward. Both intimately interact with monsoon circulations. The cause of the formation of the 30-60 day convection seesaw, however, remains unexplained.

5. Connections with the extratropics

Instability theory does not address the question of what triggers the formation of tropical TIS. Simple models (Miyahara 1987; Lau et al. 1989; Li and Wang 1992) have demonstrated that the upper-level divergence waves that travel across the western hemisphere may initiate convection over the equatorial Africa or Indian Ocean. On the other hand, the response of TIS to the effects of extratropics and subtropics has been widely recognized. Hsu et al. (1990) suggested that some intraseasonal oscillation events may be initiated by Rossby wave propagation from higher latitude into the equatorial regions. Strong equatorward flows in the western Indian Ocean and western Pacific were found to activate equatorial convection in those regions (Murakami 1987, 1988). The energy propagation or intrusion of the troughs originating from midlatitude westerlies are particularly evident in the central and eastern tropical Pacific (Liebmann and Hartmann 1984; Magana and Yanai 1991; Kiladis and Weickmann 1992).

The interaction and association between MJO and variations in midlatitude circulation were described by Weickmann (1983), Liebmann and Hartmann (1984), Weickmann et al. 1985, Lau and Phillips (1986), Ghil and Mo (1991a,b) and many others, but the connection between tropical and extratropical intraseasonal oscillation remains controversial.

6. Air-sea interaction on an intraseasonal time scale

Empirical evidences appear to suggest that air-sea interaction may be acting on the intraseasonal time scale. Krishnamurti et al. (1988) found SST variation on 30-50 day time scale on the order of 0.5-1.0°C and corresponding variation in surface latent and sensible heat fluxes with an amplitude of 40 Wm^{-2}. Further studies are needed to determine the boundary layer structure of TIS and, in particular, its relationship with underlying SST and organized convection aloft. Unfortunately, lack of oceanic observations over the western Pacific and Indian Oceans has hampered investigations of air-sea interaction on this time scale. The role of SST variation in modulation of TIS remains to be addressed.

Over the equatorial Indian Ocean evidences of coherent 30-60 day oscillations between low-level zonal wind and ocean currents, mixed layer depth, and upper thermocline temperature ware presented by McPhaden (1982). The oscillations found in the Indian ocean appear to be locally forced by surface winds (Mertz and Mysak 1984).

Significant 40-60 day variations in sea-level height (SLH) in the eastern equatorial Pacific and along the west coasts of America were detected and postulated to be remotely forced by the counterpart oscillation in the atmosphere over the western Pacific

(Enfield 1987). The coherence between the variations of low-level wind in the western Pacific and the SLH in the eastern Pacific indicates the important part of remotely-forced equatorial Kelvin waves play in the propagation of SLH signals (Erickson et al. 1983; Mitchum and Lukas 1987).

Because the initiation and termination of tropical Pacific warm events occur on a relatively short time scale of a few months, and because the rapid changes in atmospheric conditions are very likely the cause of irregularity of El Nino-Southern Oscillation (ENSO) cycle (Philander, 1990), study of the links between two major low frequency variabilities is needed for the purpose of ENSO prediction. The possible roles TIS may play in triggering Pacific warm events and some causal relationships originating from the interaction among annual cycle, MJO and ENSO were speculated (Lau and Chan 1986b; Nitta and Motoki 1987; Lau and Chan 1988). Linear instability analyses of Lau and Shen (1988) and Hirst and Lau (1990) indicated a possibility that the atmospheric moist Kelvin-wave may be destabilized by air-sea coupling if its propagation slows down to a few meters per second by precipitational heating. Hirst and Lau speculated that this unstable mode of atmospheric origin could trigger a Pacific warm event. Further studies are needed to clarify the precise role of TIS in ENSO cycle.

Our knowledge of the intraseasonal variability of the tropical atmosphere has been increased tremendously in the last two decades. An observational basis has been firmly established for various aspects of Madden-Julian oscillation and tropical intraseasonal systems. The phenomenon is viewed as far more complex today than a decade ago. Our understanding of the basic dynamics of TIS has gained a firm ground, yet many intriguing aspects of the phenomenon have not been fully explored. In view of the fact that the intraseasonal variations are linked to a variety of fundamental physical processes, a thorough understanding of the phenomenon has potential impacts on prediction of long-range variations of the tropical atmospheric circulation. Such experiments have been undertaken recently (Krishnamurti et al., 1990). Prediction of Madden-Julian oscillation is a challenge task and is expected to be one of the major breakthroughs in numerical modeling of atmospheric general circulation and climate dynamics.

Acknowledgements The author is deeply indebted to T. Li and Y. Wang for their assistance in numerical computations involved in section 5 and B. Johnson for her careful reading an earlier version of the manuscript. This work is supported by the Climate Dynamics Program, Division of Atmospheric Sciences, National Science Foundation under Grants ATM-9019315.

References

Anderson, J. R. and R. D. Rosen, 1983. J. Atmos. Sci., 41, 1584-1591.

_____, D. E. Stevens, and P. R. Julian, 1984. Mon. Wea. Rev., 112, 2431-2438.

_____, and D. E. Stevens, 1987a. J. Atmos. Sci., 44, 676-686.

_____, and D. E. Stevens, 1987b. J. Atmos. Sci., 44, 2115-2127.

Cadet, D. L., 1983. Mon. Wea. Rev., 111, 95-108.

Chang, C.-P., 1977. J. Atmos. Sci., 34, 901-910.

_____, and H. Lim, 1988. J. Atmos. Sci., 45, 1709-1720.

Chao, W.-C., 1987. J. Atmos. Sci., 44, 1940-1949.

Chen, T.-C., and M. Murakami, 1988. Mon. Wea.

Rev., 116, 892-906.

Dunkerton, T. J. and F. X. Crum, 1991. J. Meteor. Soc. Japan, 69, 449-456.

Emanuel, K. A., 1987. J. Atmos. Sci., 44, 2324-2340.

Enfield, D., 1987. J. Phys. Oceanogr., 17, 1860-1876.

Erickson, C. C., M. B. Blumenthal, S. P. Hayes, and P. Ripa, 1983. J. Phys. Oceanogr., 13, 1622-1640.

Gadgil, S. and J. Srinivasan, 1990. Meteor. Atmos. Phys., 44, 119-132.

Ghil, M., and K. Mo, 1991a. J. Atmos. Sci., 48, 752-779.

_____, and _____, 1991b. J. Atmos. Sci., 48, 780-790.

Gill, A. E., 1980. Quart. J. Roy. Meteor. Soc., 106, 447-462.

Goswami, B. N., and J. Shukla, 1984. J. Atmos. Sci., 41, 20-37.

Gutzler, D. S. and R. A. Madden, 1989. J. Atmos. Sci., 46, 641-660.

Hartmann, D. L. and M. L. Michelson, 1989. J. Atmos. Sci., 46, 2838-2862.

_____, _____, and S. A. Klein, 1992. J. Atmos. Sci., 49, 1277-1289.

Hayashi, Y., 1970. J. Meteor. Soc. Japan, 48, 140-160.

_____, and D. G. Golder, 1986, J. Atmos. Sci., 43, 3058-3067.

_____, and _____, 1988, J. Atmos. Sci., 45, 3017-3033.

_____, and S. Miyahara, 1987. J. Meteor. Soc. Japan, 65, 843-852.

Hayashi, Y. Y., and A. Sumi, 1986. Mon. Wea. Rev., 114, 605-623.

Krishnamurti, T. N. and D. Subrahmanyam, 1982. J. Atmos. Sci., 39, 2088-2095.

_____, P. K. Jayakumar, J. Sheng, N. Surgi and A Kumar, 1985. J. Atmos. Sci., 42, 364-375.

_____, D.K. Dosterhof, and A.V. Mehta, 1988. J. Atmos. Sci., 45, 1304-1322.

_____, M. Subrahmanyam, D. K. Dosterhof, and G. Daughenbaugh, 1990. Meteor. Atmos. Phys., 44, 63-83.

Lau, K.-M., and P. H. Chan, 1983. J. Atmos. Sci., 40, 2735-2750.

_____ and _____, 1985. Mon. Wea. Rev., 113, 1889-1909.

_____, and _____, 1986a. Mon. Wea. Rev., 114, 1354-1367.

_____, and _____, 1986b. Bull. Amer. Meteor. Soc., 67, 533-534.

_____, and _____, 1988. J. Atmos. Sci., 45, 506-521.

_____, and L. Peng, 1987. J. Atmos. Sci., 44, 950-972.

_____, and _____, 1990. J. Atmos. Sci., 47, 1443-1462.

_____, and T. J. Phillips, 1986. J. Atmos. Sci., 43, 1164-1181.

_____, and S. Shen, 1988. J. Atmos. Sci., 45, 1781-1797.

_____, L. Peng, C. H. Sui, and T. Nakazawa, 1989. J. Meteor. Soc. Japan, 67, 205-219.

Lau, N.-C., and K.-M. Lau, 1986. J. Atmos. Sci., 43, 2023-2047.

_____, I. M. Held, and J. D. Neelin, 1988. J. Atmos. Sci., 45, 3810-3812.

Li, T., and B. Wang, 1992. Submitted to J. Atmos. Sci..

Liebmann, B., and D. L. Hartmann, 1984. J. Atmos.

Sci., 41, 3333-3350.

Lim, H., T.-K. Lim, and C.-P. Chang, 1990. J. Atmos. Sci., 47, 3078-3091.

Lindzen, R. S., 1974. J. Atmos. Sci., 31, 156-179.

_____ and S. Nigam, 1987. J. Atmos. Sci., 44, 2440-2458.

Lorenc, A. C., 1984. Quart. J. Roy. Meteor.Soc., 110, 427-441.

McPhaden, M. J., 1982. J. Marine Res., 40, 157-176.

Madden, R. A., 1986. J. Atmos. Sci., 43, 3138-3158.

_____, and P. R. Julian, 1971. J. Atmos. Sci., 28, 702-708.

_____, and _____, 1972. J. Atmos. Sci., 29, 1109-1123.

Magana, V. and M. Yanai, 1991. J. Climate., 4, 180-201.

Mertz, J. G., and L. A. Mysak, 1984. Mon. Wea. Rev., 112, 383-386.

Mitchum, G. T. and R. Lukas, 1987. J. Phys. Oceanogr., 17, 2362-2365.

Miyahara, S., 1987. J. Meteor. Soc. Japan, 65, 341-351.

Murakami, M., 1984. J. Meteor. Soc. Japan, 62, 88-108.

Murakami, T., 1987. Mon. Wea. Rev., 115, 2134-2144.

_____, 1988. J. Climate, 1, 117-131.

_____, T. Nakazawa, and J. He, 1984. J. Meteor. Soc. Japan, 62, 440-468.

_____, and T. Nakazawa, 1985. J. Atmos. Sci., 42, 1107-1122.

_____, L.-X. Chen, and A. Xie, 1986. Mon. Wea. Rev., 114, 1456-1465.

Nakazawa, T., 1988. J. Meteor. Soc. Japan, 66, 823-839.

Neelin, J. D., I. M. Held, and H. Cook, 1987. J. Atmos. Sci., 44, 2341-2348.

Nitta, T., and T. Motoki, 1987. J. Meteor. Soc. Japan, 65, 497-506.

Philander, S. G., 1990. El Niño, La Nina, and the Southern Oscillation, Academic Press, 293 pp.

Rui, H. and B. Wang, 1990. J.Atmos. Sci., 47, 357-379.

Sikka, D. R. and S. Gadgil, 1980. Mon. Wea. Rev., 108, 1840-1853.

Smith, E. A. and A. V. Mehta, 1990. Meteor. Atmos. Phys., 44, 195-218.

Srinivasan, J., S. Gadgil, and P. J. Webster, 1991. Meteor. Atmos. Phys., 45, in press.

Swinbank, R. T., T. N. Palmer, and M. K. Davey, 1988. J. Atmos. Sci., 45, 774-788.

Takahashi, M., 1987. J. Meteor. Soc. Japan, 65, 43-49.

Wang, B., 1988a. J. Atmos. Sci., 45, 2051-2065.

_____, 1988b. J. Atmos. Sci., 45, 3521-3525.

_____, and J.-K. Chen, 1989. Quart. J. Roy. Meteor. Soc., 115, 1301-1323.

_____, and H. Rui, 1990a. Meteor. Atmos. Phys., 44, 43-61.

_____, and H. Rui, 1990b. J. Atmos. Sci., 47, 397-413.

_____, and Y. Xue, 1992. J. Atmos. Sci., 49, 549-559.

_____, and T. Li, 1993. J. Atmos. Sci., 50, in press.

Webster, P. J., 1983. J. Atmos. Sci., 40, 2110-2124.

Weickmann, K. M., 1983. Mon. Wea. Rev., 111, 1838-1858.

_____, G. R. Lusky and J. E. Kutzbach, 1985. Mon. Wea. Rev., 113, 941-960.

_____, and S. J. S. Khalsa, 1990. Mon. Wea. Rev., 118, 964-978.

Yamagata, T., and Y. Hayashi, 1984. J. Meteor. Soc. Japan, 62, 709-717.

Yasunari, T., 1979. J. Meteor. Soc. Japan, 57, 227-242.

_____, 1980. J. Meteor. Soc. Japan, 58, 225-229.

Zhu, B.-Z. and B. Wang, 1993. J. Atmos. Sci., 50, in press.